Pitx2-microRNA pathway that delimits sinoatrial node development and inhibits predisposition to atrial fibrillation

Jun Wang[a], Yan Bai[a,b,1], Na Li[a,1], Wenduo Ye[c], Min Zhang[a,b], Stephanie B. Greene[a], Ye Tao[a], Yiping Chen[c], Xander H. T. Wehrens[a,d], and James F. Martin[a,b,e,f,2]

[a]Department of Molecular Physiology and Biophysics, [f]Program in Developmental Biology, and [d]Department of Medicine, Division of Cardiology, Baylor College of Medicine, Houston, TX 77030; [e]Texas Heart Institute, Houston, TX 77030; [b]Institute of Biosciences and Technology, Texas A&M Health Science Center, Houston, TX 77030; and [c]Department of Cell and Molecular Biology, Tulane University, New Orleans, LA 70118

Edited* by Eric N. Olson, University of Texas Southwestern Medical Center, Dallas, TX, and approved May 19, 2014 (received for review April 17, 2014)

The molecular mechanisms underlying atrial fibrillation, the most common sustained cardiac arrhythmia, remain poorly understood. Genome-wide association studies uncovered a major atrial fibrillation susceptibility locus on human chromosome 4q25 in close proximity to the paired-like homeodomain transcription factor 2 (*Pitx2*) homeobox gene. *Pitx2*, a target of the left-sided Nodal signaling pathway that initiates early in development, represses the sinoatrial node program and pacemaker activity on the left side. To address the mechanisms underlying this repressive activity, we hypothesized that Pitx2 regulates microRNAs (miRs) to repress the sinoatrial node genetic program. MiRs are small noncoding RNAs that regulate gene expression posttranscriptionally. Using an integrated genomic approach, we discovered that Pitx2 positively regulates *miR-17-92* and *miR-106b-25*. Intracardiac electrical stimulation revealed that both *miR-17-92* and *miR-106b-25* deficient mice exhibit pacing-induced atrial fibrillation. Furthermore electrocardiogram telemetry revealed that mice with *miR-17-92* cardiac-specific inactivation develop prolonged PR intervals whereas mice with *miR-17-92* cardiac-specific inactivation and *miR-106b-25* heterozygosity develop sinoatrial node dysfunction. Both arrhythmias are risk factors for atrial fibrillation in humans. Importantly, *miR-17-92* and *miR-106b-25* directly repress genes, such as *Shox2* and *Tbx3*, that are required for sinoatrial node development. Together, to our knowledge, these findings provide the first genetic evidence for an miR loss-of-function that increases atrial fibrillation susceptibility.

irregular heart rate | single nucleotide variant | mouse genetics

Atrial fibrillation (AF), the most common arrhythmia in adult patients, increases in prevalence with age to almost 5% of the population over 65. Patients with AF have an increased risk of stroke, dementia, and heart failure (1). Electrical impulses that are critical for a coordinated, physiologic heartbeat originate in the sinoatrial node (SAN). In AF, abnormal fibrillatory atrial impulses override normal SAN function, with resultant irregular conduction to the ventricles. Many cases of ectopic electrical activity originate in the pulmonary vein (2). Other sites of ectopy include the left atrial posterior wall, superior vena cava, interatrial septum, crista terminalis, and coronary sinus myocardium (3, 4).

Multiple approaches have been used to uncover genes that may contribute to the AF phenotype in adult patients. A seminal genome-wide association study (GWAS), subsequently replicated by multiple studies, uncovered a single nucleotide variant (SNV) on human 4q25 that was strongly associated with familial AF (5). Patients with the 4q25 variant exhibited early onset AF that was independent from other risk factors such as hypertension and diabetes, suggesting a novel biologic mechanism involving genes located on chromosome 4q25. The presence of the 4q25 SNV also had prognostic value because patients with the SNV are prone to cardioembolic stroke and AF recurrence after ablation therapy (6, 7).

MicroRNAs (miRs) are 21- to 25-nucleotide noncoding RNAs that function in biologic processes by posttranscriptional gene silencing (8, 9). Mouse studies have revealed multiple roles for miRs in heart development (9, 10). *MiR-17-92* and its two homologous clusters, *miR-106a-363* and *miR-106b-25*, encode polycistronic miRs that are processed from a common primary miR and are grouped into different families based on their seed sequences (Fig. S1*A*) (11, 12). Germ-line *miR-17-92* loss-of-function results in heart defects including ventricular septal defects that result from abnormal differentiation of second heart field cardiac progenitors (13, 14).

Paired-like homeodomain transcription factor 2 (*Pitx2*) is the gene in closest proximity to the 4q25 SNV that has biologic relevance for AF (5). *Pitx2* is expressed on the left side of multiple organ primordia and mature organs including the heart. Within the developing heart, *Pitx2* is highly expressed in multiple sites that are prone to ectopic electrical activity, such as the left atrium, pulmonary vein, interatrial septum, crista terminalis, and left caval vein myocardium (15, 16). *Pitx2* haploinsufficient ($Pitx2^{null/+}$) adult mice are prone to AF under intracardiac electrical stimulation, revealing a direct functional connection between AF and reduced *Pitx2* levels (16, 17).

Significance

Atrial Fibrillation (AF) is the most common sustained cardiac arrhythmia in the human population. It is critical to elucidate the molecular mechanisms underlying AF, given that the prevalence of AF is expected to dramatically increase as the human population ages. We identified a microRNA (miR)-regulated genetic pathway that delimits sinoatrial node development and inhibits AF. To our knowledge, our data are the first genetic evidence showing that miR deletion results in AF predisposition. Moreover, to our knowledge, our data are the first demonstration that sinoatrial node regulatory genes are regulated by miRs. Our findings suggest attractive therapeutic targets to treat AF given that miR-based therapeutics are feasible using miR antagonists and mimics.

Author contributions: J.W., Y.B., N.L., W.Y., and J.F.M. designed research; J.W., Y.B., N.L., W.Y., S.B.G., and Y.T. performed research; Y.C. and X.H.T.W. contributed new reagents/analytic tools; J.W., Y.B., N.L., W.Y., M.Z., and J.F.M. analyzed data; and J.W., Y.B., N.L., W.Y., M.Z., and J.F.M. wrote the paper.

The authors declare no conflict of interest.

*This Direct Submission article had a prearranged editor.

Data deposition: The data reported in this paper have been deposited in the Gene Expression Omnibus (GEO) database, www.ncbi.nlm.nih.gov/geo (accession no. GSE50401).

[1]Y.B. and N.L. contributed equally to this paper.

[2]To whom correspondence should be addressed. E-mail: jfmartin@bcm.edu.

This article contains supporting information online at www.pnas.org/lookup/suppl/doi:10.1073/pnas.1405411111/-/DCSupplemental.

Here, we discovered that *miR-17-92* and *miR-106b-25* are novel downstream *Pitx2* target genes and are AF susceptibility genes. *MiR-17-92* and *miR-106b-25* inhibit the SAN genetic program in the coronary sinus and left atrium. To our knowledge, our findings are the first genetic evidence that miRs regulate SAN development and are implicated in AF predisposition.

Results

Pitx2 Positively Regulates *miR-17-92* and *miR-106b-25*. To gain insight into miRs involved in AF pathogenesis, we performed miR expression profiling using hearts from *Pitx2*$^{null/null}$ mutant and wild type, and ChIP-sequencing (ChIP-Seq) using hearts from the *Pitx2*-Flag allele (16, 18), which express Pitx2 with a C-terminal Flag epitope tag (Fig. 1 *A* and *C*). The miR profiling data at embryonic day 13.5 (E13.5) reveal that multiple individual miRs encoded by *miR-17-92* and *miR-106b-25* are reduced in *Pitx2*$^{null/null}$ mutant hearts (Fig. 1*A*). These findings are further confirmed by real-time RT-PCR (Fig. 1*B*). ChIP-Seq analysis using chromatin from adult mouse heart of the *Pitx2*^{Flag} allele (GEO accession no. GSE50401) (18) revealed that Pitx2 directly binds conserved chromatin upstream of *miR-17-92* and *miR-106b-25* (Fig. 1*C*). The Pitx2-occupied chromatin also are DNase I hypersensitive sites (ENCODE, 8-wk heart) and are occupied by p300 (ChIP-Seq data from GEO accession no. GSE32587) (19), suggesting Pitx2 actively regulates *miR-17-92* and *miR-106b-25*. The Pitx2 binding regions were further confirmed by real-time PCR using E13.5 *Pitx2*-Flag mouse heart ChIP chromatin, indicating that Pitx2 directly binds *miR-17-92* and *miR-106b-25* chromatin during embryogenesis (Fig. 1*D*). In addition, several miRs such as *miR-335* and *miR-423* were up-regulated in *Pitx2*^{null} mutant hearts (Fig. 1*A*) and ChIP-Seq data suggest that they are also potential direct Pitx2 target genes (Fig. S1 *B* and *C*).

***mir-17-92* Expression Overlaps with *Pitx2* Expression.** To determine the *miR-17-92* expression pattern in heart, we generated an *miR-17-92* bacterial artificial chromosome transgenic LacZ reporter line (20) and compared it with a *Pitx2* LacZ knock-in allele (16). In E12.5 hearts, LacZ staining indicated that *miR-17-92* is expressed in the outflow tract (OFT), left atrium (LA), coronary sinus, and atrioventricular canal (Fig. S2 *A–C*), where *Pitx2* is also endogenously expressed (Fig. S2 *D–F*). Together, these data indicate that *miR-17-92* and *Pitx2* have overlapping expression domains.

***miR-17-92* and *miR-106b-25* Mutant Mice Have Normal Baseline Electrophysiological Parameters.** We analyzed baseline cardiac electrophysiological parameters of *miR-17-92* and *miR-106b-25* deficient adult mice. Four genotypes including wild-type, *miR-17-92*$^{null/+}$, *miR-106b-25*$^{null/+}$, and *miR-106b-25*$^{null/null}$ mice were studied. Only *miR-17-92*$^{null/+}$ adult mice were compared in the study because *miR-17-92*$^{null/null}$ mutants are embryonic lethal. For each genotype, we evaluated heart rate (HR), the interval from the beginning of the P wave to the peak of the R wave (PR), the duration of the interval between the beginning of the Q wave to the peak of the S wave (QRS), the duration of the Q-T interval corrected for the heart rate atrial effective refractory period (QTc), the sinus node recovery time (SNRT), atrial effective refractory period (AERP), and the atrioventricular nodal effective refractory period (AVERP) (Table S1).

All baseline electrophysiologic parameters were similar in *miR-17-92*$^{null/+}$, *miR-106b-25*$^{null/+}$, and *miR-106b-25*$^{null/null}$ mice compared with wild-type mice. There were no episodes of spontaneous AF observed in any studied mice.

***miR-17-92* and *miR-106b-25* Deficient Mice Are Susceptible to Pacing-Induced Atrial Fibrillation.** To evaluate whether the loss of *miR-17-92* and *miR-106b-25* increases susceptibility to AF initiation, we performed intracardiac electrical stimulation studies. An overdriving pacing protocol was used to induce AF, and three pacing trials were applied in each mouse. Simultaneous surface ECG and intracardiac electrograms revealed absent P-waves and irregular R-wave to R-wave (RR) intervals in *miR-17-92* $^{null/+}$ (Fig. 2*B*) and *miR-106b-25*$^{null/null}$ (Fig. 2*D*) mice after burst pacing, which are suggestive of AF. In contrast, wild-type (Fig. 2*A*) and *miR-106b-25*$^{null/+}$ (Fig. 2*C*) mice showed sinus rhythm instead of reproducible AF following rapid pacing.

MiR-17-92 $^{null/+}$ and *miR-106b-25*$^{null/null}$ showed a much higher incidence of reproducible pacing-induced AF: 57.4% of *miR-17-92* $^{null/+}$ mice (4 of 7) and 83.3% of *miR-106b-25*$^{null/null}$ mice (5 of 6) had reproducible pacing-induced AF after atrial pacing whereas 14.3% of *miR-106b-25*$^{null/+}$ (1 of 8) and no wild-type (0 of 8) exhibited reproducible AF (Fig. 2*E*). Moreover, we quantified the duration of the longest AF episode in each tested animal and compared the differences between different genotypes. The *miR-17-92* $^{null/+}$ and *miR-106b-25*$^{null/null}$ mice also developed significantly longer duration of inducible AF compared with wild-type mice (Fig. 2*F*). Taken together, our findings

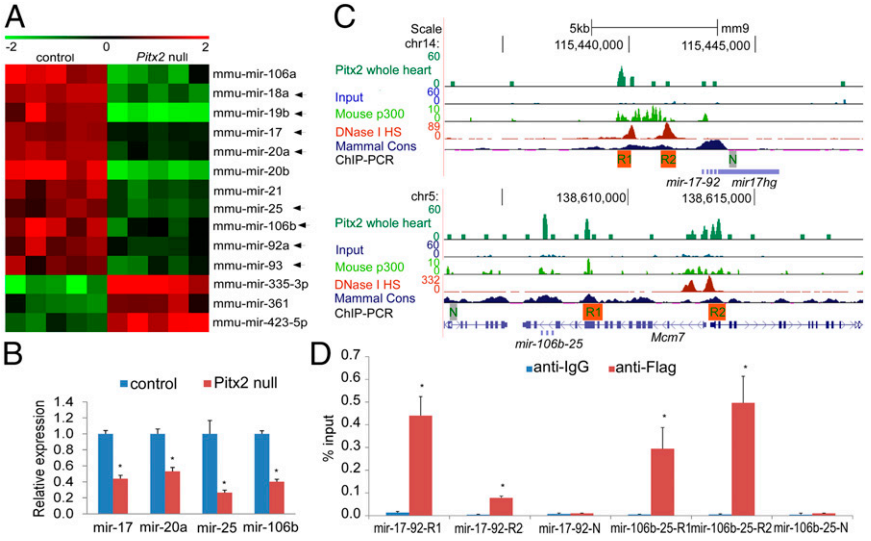

Fig. 1. Pitx2 positively regulates *miR-17-92* and *miR-106b-25*. (*A*) Heat map of miR array with wild-type control and *Pitx2*-null mutant hearts at E13.5. Arrows designate individual miRs from *mir-17-92* and *mir-106b-25*. (*B*) Real-time PCR validation of miR array data at E13.5. **P* < 0.05. (*C*) Three-month-old mouse whole-heart ChIP-Seq enrichment profiles (GSE50401) (18) for Pitx2-bound loci at upstream of *miR-17-92* and *miR-106b-25*. The peaks from different datasets including Pitx2 ChIP-Seq, input track, P2 mouse heart p300 ChIP-Seq (GSE32587) (19), and 8-wk-old heart DNase I Hypersensitive Site (HS) Seq (ENCODE), as well as mammal conservation (cons) track, are aligned for comparison. Locations of real-time PCR validation of ChIP enrichment are indicated under datasets. For Pitx2 ChIP-Seq, input, and P300 ChIP-Seq, the scale indicates read count that was normalized to 10 million reads. For the DNase I HS track, we used the ENCODE default scale. N, negative control; R1, region1; R2, region 2. (*D*) In vivo real-time ChIP PCR indicated that *miR-17-92* and *miR-106b-25* were bound by Pitx2 in E13.5 mouse hearts.

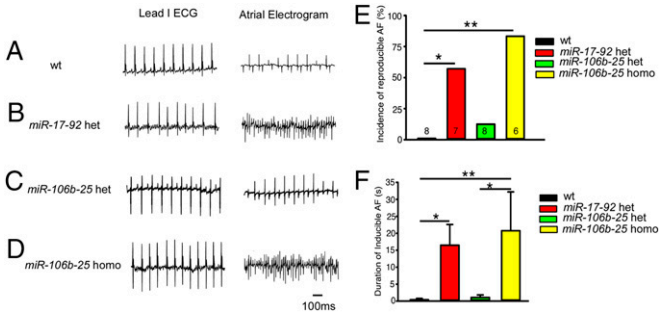

Fig. 2. *MiR-17-92* and *miR-106b-25* deficient mice are susceptible to atrial fibrillation. Simultaneous recordings of simultaneous surface ECG (lead I) and intracardiac electrograms in wild-type (wt) (*A*), *miR-17-92* $^{null/+}$ (*miR-17-92* het) (*B*), *miR-106b-25* $^{null/+}$ (*miR-106b-25* het) (*C*), and *miR-106b-25*$^{null/null}$ (*miR-106b-25* homo) (*D*) mice after burst pacing. Absent P-waves and irregular RR intervals suggest pacing-induced AF in *miR-17-92* het (*B*) and *miR-106b-25* homo (*D*) mice. (*E*) The incidence of inducible AF in different genotypes compared with wt mice are summarized in the bar graph. (*F*) The duration of the longest inducible AF episode in different genotypes compared with wt mice is summarized in the bar graph. $*P < 0.05$, $**P < 0.01$.

indicate that loss of *miR-17-92* and *miR-106b-25,* like *Pitx2*, increases susceptibility to AF.

Sinoatrial-Node Dysfunction in Mice with *miR-17-92* Cardiac-Specific Knockout and *miR-106b-25* Haploinsufficiency. To determine whether compound mutants for *miR-17-92* and *miR-106b-25* develop atrial arrhythmias, we conditionally inactivated *miR-17-92* using the *Nkx2.5 Cre* driver that directs cre activity in heart. Continuous ambulatory ECGs were recorded using telemetry in mice aged from 6 wk to 4 mo old. We first evaluated *Nkx2.5*^{Cre}*;miR-17-92*$^{flox/flox}$ adult mice and found that they all had prolonged PR intervals or first-degree atrioventricular (AV) block (Fig. 3*F*, $n = 6$), which is an AF risk factor in the human population (1). Importantly, long-term follow-up of patients in the Framingham cohort found that prolonged PR interval commonly progressed to more severe arrhythmias requiring pacemaker implantation that included SAN dysfunction, high-grade AV block, and AF (1).

The *Nkx2.5*^{Cre}*;miR-17-92*$^{flox/flox}$*;miR-106b-25*$^{null/null}$ double mutant mice were runted, for reasons that are under investigation and could not be used for these studies. However, *Nkx2.5*^{Cre}*;miR-17-92*$^{flox/flox}$*;miR-106b-25*$^{null/+}$ ($n = 10$) mice developed SAN dysfunction, also called sick-sinus syndrome, which was revealed by irregular sinus rhythm with low amplitude P waves and variable ventricular response (Fig. 3*B*). SAN dysfunction, which frequently coexists with AF in human patients (21), is a known AF risk factor (22) and significantly associated with prolonged atrial fibrillatory cycle length (23). Both 6-wk-old ($n = 4$) and 4-mo-old ($n = 6$) *Nkx2.5*^{Cre}*;miR-17-92*$^{flox/flox}$*;miR-106b-25*$^{null/+}$ mice had SAN dysfunction, with more frequent and longer arrhythmias in 4-mo-old mice. Moreover, some 4-mo-old *Nkx2.5*^{Cre}*;miR-17-92*$^{flox/flox}$*;miR-106b-25*$^{null/+}$ mice had, in addition to SAN dysfunction, type 2 second-degree atrioventricular block (AV block) (3 out of 6) (Fig. 3*C*). Together these data suggest that progressive removal of *miR-17-92* and *miR-106b-25* complexes results in atrial arrhythmias of increasing severity that in human patients are known AF risk factors. Moreover, our findings support the hypothesis that *miR-17-92* and *miR-106b-25* have overlapping functions in atrial homeostasis. Notably, the *Nkx2.5*^{Cre}*;miR-17-92*$^{flox/flox}$*;miR-106b-25*$^{null/+}$ failed to develop sustained AF perhaps because of the presence of the single allele of *miR-106b-25*.

Because it has been reported that aged *Nkx2.5*^{Cre} mice have background-dependent phenotypes including arrhythmias (24), we performed a number of control experiments. Importantly, SAN dysfunction was not observed in mice of other genotypes including wild-type (6 wk old, $n = 4$) (Fig. 3*A*), *Nkx2.5*^{Cre} (6 wk old, $n = 4$; 4 mo old, $n = 4$) (Fig. 3*D*), *miR-17-92*$^{flox/flox}$*; miR-106b-25*$^{null/+}$ (6 wk old, $n = 4$; 4 mo old, $n = 4$) (Fig. 3*E*), and *Nkx2.5*^{Cre}*; miR-17-92*$^{flox/flox}$ (6 wk old, $n = 3$; 4 mo old, $n = 3$) (Fig. 3*F*). In addition, one 4-mo-old *Nkx2.5*^{Cre} mice had prolonged PR interval that is similar as detected in 6-wk-old *Nkx2.5*^{Cre}*; miR-17-92*$^{flox/flox}$ mice.

Normal Cardiac Structure in Mice with *miR-17-92* Cardiac-Specific Knockout and *miR-106b-25* Haploinsufficiency. To examination whether the cardiac arrhythmias in *Nkx2.5*^{Cre}*; miR-17-92*$^{flox/flox}$*; miR-106b-25*$^{null/+}$ mice were caused by cardiac structural abnormalities, we first did echocardiography to examine the cardiac function of *Nkx2.5*^{Cre}*; miR-17-92*$^{flox/flox}$*; miR-106b-25*$^{null/+}$ mutants ($n = 6$) compared with *miR-17-92*$^{flox/flox}$*; miR-106b-25*$^{null/+}$ and *Nkx2.5*^{Cre} controls (*miR-17-92*$^{flox/flox}$*; miR-106b-25*$^{null/+}$, $n = 4$; *Nkx2.5*^{Cre} $n = 3$). Compared with control mice, no obvious changes in cardiac contractile function, dimension and wall thickness were found in *Nkx2.5*^{Cre}*; miR-17-92*$^{flox/flox}$*; miR-106b-25*$^{null/+}$ mutant mice at the age of 4 mo (Fig. S3 and Table S2). We also performed hematoxylin/eosin (H&E) staining in *Nkx2.5*^{Cre}*; miR-17-92*$^{flox/flox}$*; miR-106b-25*$^{null/+}$ mutants ($n = 10$) and *miR-17-92*$^{flox/flox}$*; miR-106b-25*$^{null/+}$ control mice ($n = 4$) at the age of 4 mo. We didn't detect any obvious defect of cardiac structure in *Nkx2.5*^{Cre}*; miR-17-92*$^{flox/flox}$*; miR-106b-25*$^{null/+}$ mutants ($n = 10$) compared with *miR-17-92*$^{flox/flox}$*; miR-106b-25*$^{null/+}$ controls ($n = 4$) (Fig. S4 *A* and *B*) except for one mutant that had a small membranous ventricular septal defect. There were no atrial septal defects and no evidence for atrial enlargement in the *Nkx2.5*^{Cre}*; miR-17-92*$^{flox/flox}$*; miR-106b-25*$^{null/+}$ mutants either histologically or by measuring atrial weights (Fig. S4 *A*, *B*, and *J*). These findings are consistent with a recent report from Chen et al., who also didn't find structure changes in *Nkx2.5*^{Cre}*; miR-17-92*$^{flox/flox}$ mutant mice (25).

Wheat germ agglutinin (WGA) staining data indicated that there was no obvious change in cardiomyocyte cell size of ventricular myocardium of *Nkx2.5*^{Cre}*; miR-17-92*$^{flox/flox}$*; miR-106b-25*$^{null/+}$ mutants ($n = 3$) compared with *miR-17-92*$^{flox/flox}$*; miR-106b-25*$^{null/+}$ controls ($n = 3$) at 4 mo old (Fig. S4 *C–E*). Notably, although Chen et al. found that 10-mo-old *Nkx2.5*^{Cre}*; miR-17-92*$^{flox/flox}$ mutant mice exhibited cardiomyocyte hypertrophy (25), we did not detect such changes in younger mice. Masson's Trichrome staining was used to detect the

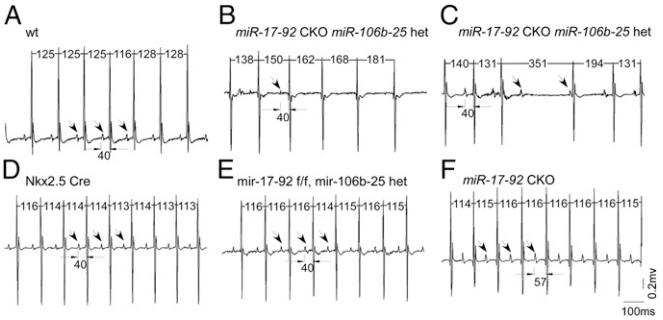

Fig. 3. Mice with *miR-17-92* cardiac-specific knockout and *miR-106b-25* haploinsufficiency have spontaneous arrhythmias. Continuous ambulatory ECGs were recorded in mice using telemetry. Arrows designate measured PR intervals. Continuous ambulatory ECGs indicated SAN dysfunction in a 6-wk-old *Nxk2.5*^{Cre}*; miR-17-92*$^{flox/flox}$*; miR-106b-25*$^{null/+}$ (*miR-17-92* CKO *miR-106b-25* het) mouse (*B*) but not in WT mouse (*A*), *Nxk2.5*^{Cre} (*D*) *miR-17-92*$^{flox/flox}$*; miR-106b-25*$^{null/+}$ (*E*), and *Nxk2.5*^{Cre}*; miR-17-92*$^{flox/flox}$ (*F*). Although no episode of SAN dysfunction was detected, *Nxk2.5*^{Cre}*; miR-17-92*$^{flox/flox}$ showed prolonged PR intervals. Four-month-old *miR-17-92* CKO *miR-106b-25* het mice had not only SAN dysfunction, but also type 2 second-degree atrioventricular block (an example shown in *C*). RR interval and PR interval measurements are labeled, and arrows designate P waves.

level of fibrosis, which revealed no significant difference between *Nkx2.5*^{Cre}*; miR-17-92*$^{flox/flox}$*; miR-106b-25*$^{null/+}$ mutants (n = 3) and *miR-17-92*$^{flox/flox}$*; miR-106b-25*$^{null/+}$ controls (n = 3) (Fig. S4 *F–I*). Moreover, we evaluated the ratio of atrial weight to body weight (AW/BW) in *Nkx2.5*^{Cre}*; miR-17-92*$^{flox/flox}$*; miR-106b-25*$^{null/+}$ mutants (n = 4) compared with *miR-17-92*$^{flox/flox}$*; miR-106b-25*$^{null/+}$ and *Nkx2.5*^{Cre} controls (*Nkx2.5*^{Cre}, n = 3; *miR-17-92*$^{flox/flox}$*; miR-106b-25*$^{null/+}$, n = 3) and found there was no significant difference in AW/BW between mutants and controls (Fig. S4*J*). Taken together, we conclude that there were no obvious cardiac structural defects in all but one of the 4-mo-old *Nkx2.5*^{Cre}*; miR-17-92*$^{flox/flox}$*; miR-106b-25*$^{null/+}$ mutants.

miR-17-92 Represses Shox2 and Tbx3. The short stature homeobox gene *Shox2* and T-Box gene *Tbx3*, SAN gene program components, are required for normal SAN development (26, 27). Whole-mount in situ hybridization followed by transverse sections through inflow of the heart revealed that *Shox2* expression is up-regulated in left superior caval vein and coronary sinus of *miR-17-92*$^{null/null}$ mutants (Fig. 4 *A* and *B* and Fig. S5 *A* and *B*). Immunofluorescence data using a Shox2 antibody also indicated the up-regulation of *Shox2* expression in *miR-17-92*$^{null/null}$ mutant left superior caval vein (Fig. S5 *I–L*) compared with wild-type control (Fig. S5 *E–H*). *Tbx3,* that enables SAN myocardium to separate from working atrial myocardium is expanded and up-regulated in the left atrioventricular canal of *miR-17-92*$^{null/null}$ mutant whereas *Tbx3* expression is more prominent in the right atrioventricular canal of wild-type controls (Fig. 4 *C* and *D* and Fig. S5 *C* and *D*). To quantify the expression level of *Shox2* and *Tbx3* in *miR-17-92*$^{null/null}$ mutants compared with wild type, whole-heart total RNA were isolated for quantitative RT-PCR (qRT-PCR). qRT-PCR data revealed significant *Shox2* and *Tbx3* up-regulation in *miR-17-92* mutants compared with wild type (Fig. 4*E*).

***miR-17-92* and *miR-106b-25* Directly Regulate *Shox2* and *Tbx3*.** The *Shox2* 3′ UTR contains conserved *miR-17/20a/106b* family seed sequence (Fig. S6*A*), and the *Tbx3* 3′ UTR contains both a conserved *miR-17/20a/106b* family seed site and a conserved *miR-92a/25* family seed site (Fig. S6 *B* and *C*). We constructed luciferase reporter plasmids with the 3′ UTRs of *Shox2* and *Tbx3* to test whether those miR seed sites function in vitro. There are drastic reductions in luciferase activity for both *Shox2* and *Tbx3* luciferase reporters when cotransfected with respective miR mimics (Fig. 4 *F* and *G* and Fig. S6 *D* and *E*). When we mutate the respective miR seed sites within the 3′ UTRs of *Shox2* and *Tbx3*, the repression caused by the corresponding miR is ablated (Fig. 4 *F* and *G* and Fig. S6 *D* and *E*).

Given that *Shox2* 3′ UTR contains four conserved seed sites of different miRs/miR families (Fig. S7*A*) and that only *miR-17* family is expressed in the embryonic heart whereas the other miRs/miR families are barely detectable (Fig. S7*B*), we hypothesized that *miR-17* family exerts the dominant miR regulation on the *Shox2* 3′ UTR. To obtain genetic evidence supporting *Shox2* regulation by *miR-17* family, we generated a *Shox2a*^{HA} knock-in allele that replaced the endogenous 3′ UTR with a heterologous 3′ UTR to release *Shox2* expression from endogenous miR regulation. Notably the *Shox2a*^{HA} allele still keeps the majority of endogenous transcriptional regulatory sequences, including intron 2 that contains a Pitx2 binding region (Fig. 4 *H* and *I*, Fig. S8*A*, *Methods*, and *SI Methods*). Homozygous *Shox2a*^{HA} mice (*Shox2a*$^{HA/HA}$) are neonatal lethal: 81.25% (13 out 16 from nine litters) of *Shox2a*$^{HA/HA}$ mice die within postnatal day1 without obvious morphological defects. To determine whether *Shox2* expression is expanded in the *Shox2a*$^{HA/HA}$ embryos, we performed immunofluorescence studies with a Shox2 antibody. At E16.5, *Shox2* is highly expressed in interatrial septum of *Shox2a*$^{HA/HA}$ (Fig. 4 *N–Q*) but not in wild type (Fig. 4 *J–M*). Moreover, expression of *Shox2* in SAN is dramatically higher in *Shox2a*$^{HA/HA}$

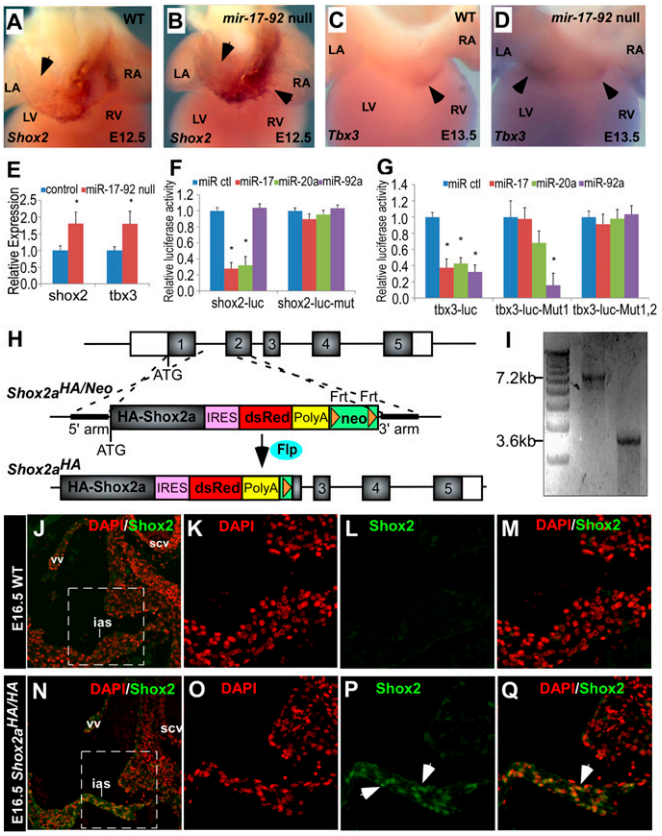

Fig. 4. *MiR-17-92* directly represses *Shox2* and *Tbx3*. (*A–D*) Whole-mount in situ hybridization with indicated probes in embryonic mouse hearts. Black arrows designate expression pattern. (*E*) qRT-PCR data indicate that expression of *Shox2* and *Tbx3* elevate in *miR-17-92* knockout mutants. (*F* and *G*) Luciferase reporter assays with reporters and miRs as labeled. Mean ± SEM, $*P < 0.05$. (*H*) Schematic diagram of *Shox2a*^{HA} allele. The mouse *Shox2* gene contains six exons as indicated by numbered blocks (coding sequence indicated in gray and noncoding sequence indicated in white). Partial of the endogenous *Shox2* sequence was replaced by DNA sequence encoding N-terminal FLAG-HA-tagged, full-length *Shox2a*, IRES-DsRed, SV40 early polyA signal and Frt flanking neomycin-resistance cassette driven by PGK promoter (neo), which is named *Shox2a*$^{HA/Neo}$ allele. Neo is further removed by crossing with germ-line Flp deleter strain to obtain *Shox2a*^{HA} allele. (*I*) Long range PCR showing targeted clones of *Shox2a*$^{HA/Neo}$ allele. Forward primer on 5′ flanking region out of the 5′ homology arm and reverse primer on DsRed yield a 7.2-kb band; forward primer on neo and reverse primer on 3′ flanking region out of 3′ homology arm yield a 3.6-kb band. (*J–Q*) Immunofluorescence shows *Shox2* is highly expressed in E16.5 atrial septum of *Shox2a*$^{HA/HA}$ embryos but not in wild-type embryos. Boxed areas in *J* and *N* are correspondingly shown at higher magnification in *K–M* and *O–Q*. Nuclei (red) stained with DAPI. White arrows designate Shox2-expressing cells. ias, interatrial septum; scv, surperior caval vein; vv, venous valve.

(Fig. S8 *D* and *E*) compared with wild type (Fig. S8 *B* and *C*). Although we cannot exclude the possibility that other features of the *Shox2*^{HA} allele, such as loss of splicing, may contribute to its abnormal expression, our findings are consistent with *Shox2* regulation by *miR-17-92*.

In addition, we further performed in situ hybridization in E12.5 *miR-17-92*$^{null/null}$ mutants and wild-type controls using *Bmp4* probe, which was previously shown as a downstream target of Shox2 (28). The in situ hybridization and heart-sectioning data indicated that *Bmp4* expression is up-regulated in *miR-17-92*$^{null/null}$ mutants (Fig. S9 *D–F*) in a similar pattern of *Shox2* up-regulation in *miR-17-92*$^{null/null}$ mutants. *Bmp4* is highly expressed in the left superior caval vein and coronary sinus of *miR-17-92*$^{null/null}$ mutants (Fig. S9 *D–F*) whereas it is only moderately expressed in

the coronary sinus of wild-type controls (Fig. S9 *A–C*). Together, these data further support the model that the *miR-17-92* and *miR-106b-25* directly inhibit *Shox2*.

Discussion

The SAN develops from a larger pool of competent cells that is progressively refined through the function of important developmental regulatory genes such as *Pitx2*. Progenitors within the sinus venosus give rise to sinus horn myocardium and SAN myocardium. In chick, discrete cells within lateral plate also contribute to the pacemaker (29). Recent work indicates that a dominant pacemaker activity is found in the E8.5 left inflow tract, where *Pitx2c* is expressed, but switches to the right SAN by E12.5 (15, 30). Our data are consistent with the notion that *Pitx2* directly regulates this developmental switch in part by regulating *miR-17-92* and *miR-106b-25*.

Our findings indicate that *miR-17-92* and *miR-106b-25* directly target SAN genes *Shox2* and *Tbx3*. Previous studies have shown that both *Shox2* and *Tbx3* promote SAN specification while inhibiting working myocardium specification. Although *Shox2* is required for SAN development in mice, it has not yet been implicated in human heart disease. However, there are data indicating that *Shox2* is a target for *Tbx5* that has been implicated in human AF and prolonged PR interval through GWAS studies (31, 32). *Tbx3* has also been implicated in human PR interval prolongation in GWAS studies (32) and induces pacemaker properties in adult myocardium when misexpressed (33). Other than the novel targets we identified here, *miR-17-92* and *miR-106b-25* have other targets. A transgenic mouse study using conditional *miR-17-92* overexpression suggested that *miR-17-92* directly targets *Pten* and *Cx43* (34). It will be necessary to investigate other *miR-17-92* target genes to thoroughly understand these two miR clusters in AF.

Mutations in miRs have not yet been uncovered in AF patients. Before our study, genetic loss-of-function studies in mice have failed to show a requirement for miRs in AF. A number of profiling studies suggested potential roles for miRs in AF. For example, *miR-328* expression was elevated in human AF patients and in a canine AF model although direct functional analysis of *miR-328* awaits further experimentation (35). *MiR-21* expression was increased in AF patients, a mouse model of spontaneous AF, and age-induced atrial fibrosis whereas *miR-21* knockdown suppressed atrial fibrosis and AF promotion in rats (36, 37). A recent report indicated that *miR-29b* plasma levels were decreased in patients with AF or congestive heart failure (38). Similarly, *miR-26* was down-regulated in the atria of an AF dog model, and experimental *miR-26* knockdown reproduced AF-induced fibroblast activation, a central event in AF-promoting remodeling (39). Expression of *miR-26* family members was reduced in human AF patients, and *Kcnj2* was shown to be a direct *miR-26* target. Moreover, *miR-26* transcription was repressed by nuclear factor of activated T cells making a direct connection between calcium signaling and *miR-26* in AF (40).

Experiments looking at *miR-17-92* showed that *miR-19a* expression was reduced in serum of patients with persistent AF (41). In patients with AF and mitral stenosis, several individual members of the *miR-17-92* cluster, including *miR-17, miR-19a, miR-19b*, and *miR-20a,* were significantly down-regulated compared with healthy individuals (42). Cardiac and smooth-muscle conditional overexpression of *miR-17-92* in mice developed dilated, hypertrophic cardiomyopathy with arrhythmias (34). Our data along with the human expression data indicate that loss-of-function of all miRs in the *miR-17-92* cluster predisposes to AF, suggesting that both loss and gain of *miR-17-92* may stimulate cardiac arrhythmias.

The *Nkx2.5^{Cre};miR-17-92$^{flox/flox}$* mutant mice showed prolonged PR interval whereas the *Nkx2.5^{Cre};miR-17-92$^{flox/flox}$;miR-106b-25$^{null/+}$* mutants had a more severe phenotype, including SAN node dysfunction and second degree AV block, suggesting functional redundancy between *miR-17-92* and *miR-106b-25*. These phenotypes are likely to be part of a continuous clinical spectrum of conduction disorders in human patients. Data from the Framingham study have shown that many patients that initially present with prolonged PR, also called first-degree AV block, commonly progress to SAN dysfunction with higher-degree AV block. These patients also commonly progress to atrial fibrillation (1). Moreover, a recent report revealed that *miR-25* regulates calcium handling by directly regulating *Serca2* in adult heart failure (43), suggesting that *miR-17-92* and *miR-106b-25* function in adult calcium homeostasis. Our data along with recent findings suggest that *miR-17-92* and *miR-106b-25* have multiple gene targets that function at different stages of AF predisposition.

Previous studies revealed that Pitx2 directly represses *Shox2* in left inflow tract working myocardium. We have now found that this repressive mechanism also includes *Shox2* repression by Pitx2-regulated miRs *miR-17-92* and *miR-106b-25*. Both *Tbx3* and *Shox2* expression domains were expanded in *Pitx2 $^{null/+}$* and *Pitx2 $^{null/null}$* mutant embryos. The working model that we previously developed (16) holds that *Pitx2* functions within a gene regulatory network (GRN) on the left side of the inflow tract to directly repress *Shox2* and the SAN genetic program in left atrium and left caval veins.

Our results, indicating that *Pitx2* directly transactivates *miR-17-92* and *miR-106b-25* transcription, uncover a developmental *Pitx2-miR* pathway that suppresses AF predisposition. The finding that *miR-17-92* and *miR-106b-25* deficient mice are prone to AF and directly repress the SAN regulatory genes *Shox2* and *Tbx3* further supports our model (Fig. S10). The notion that ectopic expression of the SAN genetic program can contribute to AF predisposition is an important area for future study. Moreover, it is likely that this proposed developmental mechanism works together with other mechanisms, such as defective calcium handling, in AF predisposition. Although reduced *Pitx2* levels have been observed in some adult human AF patients, *Pitx2* also functions during development. In addition, recent findings indicate that *Pitx2* mRNA levels are elevated in some patients that are in active AF at the time of tissue collection, indicating that *Pitx2* transcriptional regulation is complex and requires further study (44). Because our work is limited to rodent studies, definitive insight into the role of *miR-17-92* and *miR-106b-25* in human AF await further human genetic studies.

Methods

See details in *SI Methods*.

Mouse Alleles and Transgenic Lines. The *Pitx2^{Flag}*, *miR-17-92*–null, *miR-17-92* Flox, *miR-106b-25*–null, and *Nkx2.5^{Cre}* alleles were previously described (14, 24, 16). To generate the *Shox2^{HA}* allele, which is free of endogenous 3′ UTR regulation, we replaced part of the endogenous *Shox2* sequence with a *Flag-HA-mouseShox2a-DsRed-polyA* sequence that included an Frt flanked neomycin-resistance cassette (Fig. 4*E*) in G4 embryonic stem (ES) cells (45). G418 selected ES clones were screened by long-range PCR followed by sequencing of PCR products. Targeted clones showed a 7.2-kb band and a 3.6-kb band on gel (Fig. 4*F*). Correctly targeted clone was injected into blastocysts to create chimera mice. Chimeras were crossed with CD-1 females (Charles River) to generate F1 mice and were subsequently genotyped by long-range PCR.

Chromatin Immunoprecipitation, ChIP-Sequencing, and ChIP-Seq Analysis. E13.5 hearts were collected from *Pitx2^{Flag}* allele and followed by ChIP analysis as previously described (16), and DNA obtained from ChIP were used for real-time PCR to quantify enrichment. ChIP-Seq was performed using 3-mo-old mouse whole hearts of *Pitx2^{Flag}* allele, and data are available through the Gene Expression Omnibus (GEO) data repository under accession number GSE50401 (18). For ChIP-Seq analysis, Ion torrent PGM reads were aligned to the mm9 (NCBI Build 37) assembly using Torrent Suite (2.0.1) Ion-alignment (2.0.3–1). A total 1.9 million reads were uniquely mapped to mouse genome mm9. Total reads from input were 1.29×10^7. ChIP-Seq peaks were called using Homer package using

threshold FDR effective Poisson 3.7×10^{-8}, minimum read number 5. Then, 12,417 significant peaks were called; 8.97% of the reads were enriched in significant peaks. The ChIP-Seq data were converted to bedGraph file and visualized in the University of California, Santa Cruz genome browser. The total read number was normalized to 10 million; therefore, the *y* axis value indicated the normalized number of reads in a 10-bp window. The Pitx2 ChIP-Seq dataset was also aligned to postnatal day 2 (P2) mouse heart p300 ChIP-Seq (GSE32587) (19) and 8-wk-old mouse heart DNase I Hypersensitive Site Seq (ENCODE) datasets to show correlation.

Transthoracic Echocardiography. Mice were anesthetized using 1.5% (vol/vol) isoflurane mixed with 95% (vol/vol) O_2 and placed on a heated platform where all four limbs were taped to copper ECG electrodes. Cardiac function was assessed using a VisualSonics VeVo 770 Imaging System (VisualSonics) equipped with a high-frequency 30-MHz probe, as described (46).

Cardiac Electrophysiology. In vivo electrophysiology in mice was conducted as previously described (47). Briefly, intracardiac electrograms were recorded using a 1.1F octapolar catheter (EPR-800; Millar Instruments) inserted via the right jugular vein. Atrial fibrillation (AF) inducibility was determined by previous protocol (48) and defined as overdriving pacing and defined as the occurrence of rapid and fragmented atrial electrograms with irregular AV-nodal conduction and ventricular rhythm for at least 1 s. Three pacing trials were applied in each mouse. Inducibility of AF was considered positive if at least two of three pacing trials induced AF. Moreover, ambulatory ECGs were recorded in mice using telemetry transmitters (Data Sciences International) as previously described (49). Briefly, telemetry transmitters were implanted in the abdominal cavity of mice with s.c. electrodes in a lead II configuration. ECGs were continuously recorded by telemetry using Dataquest software, version 4.1 (Data Sciences International) and analyzed using Dataquest software.

ACKNOWLEDGMENTS. This work was supported by a 2012–2013 Michael Bilitch Fellowship in Cardiac Pacing and Electrophysiology from the Heart Rhythm Society (to J.W.), American Heart Association (AHA) Grant 12PRE11720003 (to Y.B.), AHA Grant 12BGIA12050207 (to N.L.), AHA Grant 13PRE13750003 (to W.Y.), National Institutes of Health (NIH) Grant 1F32HL105041 (to Y.T.), AHA Grant 13EIA14560061, NIH Grants R01-HL089598 and R01-HL091947, the Fondation Leducq Alliance for CaMKII Signaling in Heart (X.H.T.W.), NIH Grant 5R01HL118761 (to J.F.M.), NIH Grant R01DE17792 (to Y.C.), and the Vivian L. Smith foundation (J.F.M.).

1. Cheng S, et al. (2009) Long-term outcomes in individuals with prolonged PR interval or first-degree atrioventricular block. *JAMA* 301(24):2571–2577.
2. Haïssaguerre M, et al. (1998) Spontaneous initiation of atrial fibrillation by ectopic beats originating in the pulmonary veins. *N Engl J Med* 339(10):659–666.
3. Katritsis DG, et al. (2004) Conduction patterns in the cardiac veins: Electrophysiologic characteristics of the connections between left atrial and coronary sinus musculature. *J Interv Card Electrophysiol* 10(1):51–58.
4. Lin WS, et al. (2003) Catheter ablation of paroxysmal atrial fibrillation initiated by non-pulmonary vein ectopy. *Circulation* 107(25):3176–3183.
5. Gudbjartsson DF, et al. (2007) Variants conferring risk of atrial fibrillation on chromosome 4q25. *Nature* 448(7151):353–357.
6. Husser D, Adams V, Piorkowski C, Hindricks G, Bollmann A (2010) Chromosome 4q25 variants and atrial fibrillation recurrence after catheter ablation. *J Am Coll Cardiol* 55(8):747–753.
7. Bellenguez C, et al.; International Stroke Genetics Consortium (ISGC); Wellcome Trust Case Control Consortium 2 (WTCCC2) (2012) Genome-wide association study identifies a variant in HDAC9 associated with large vessel ischemic stroke. *Nat Genet* 44(3):328–333.
8. Bartel DP (2009) MicroRNAs: Target recognition and regulatory functions. *Cell* 136(2): 215–233.
9. van Rooij E, Olson EN (2007) MicroRNAs: Powerful new regulators of heart disease and provocative therapeutic targets. *J Clin Invest* 117(9):2369–2376.
10. Montgomery RL, et al. (2011) Therapeutic inhibition of miR-208a improves cardiac function and survival during heart failure. *Circulation* 124(14):1537–1547.
11. Concepcion CP, Bonetti C, Ventura A (2012) The microRNA-17-92 family of microRNA clusters in development and disease. *Cancer J* 18(3):262–267.
12. Mendell JT (2008) miRiad roles for the miR-17-92 cluster in development and disease. *Cell* 133(2):217–222.
13. Wang J, et al. (2010) Bmp signaling regulates myocardial differentiation from cardiac progenitors through a MicroRNA-mediated mechanism. *Dev Cell* 19(6):903–912.
14. Ventura A, et al. (2008) Targeted deletion reveals essential and overlapping functions of the miR-17 through 92 family of miRNA clusters. *Cell* 132(5):875–886.
15. Liu C, et al. (2002) Pitx2c patterns anterior myocardium and aortic arch vessels and is required for local cell movement into atrioventricular cushions. *Development* 129(21): 5081–5091.
16. Wang J, et al. (2010) Pitx2 prevents susceptibility to atrial arrhythmias by inhibiting left-sided pacemaker specification. *Proc Natl Acad Sci USA* 107(21):9753–9758.
17. Kirchhof P, et al. (2011) PITX2c is expressed in the adult left atrium, and reducing Pitx2c expression promotes atrial fibrillation inducibility and complex changes in gene expression. *Circ Cardiovasc Genet* 4(2):123–133.
18. Tao Y, et al. (2014) Pitx2, an atrial fibrillation predisposition gene, directly regulates ion transport and intercalated disc genes. *Circ Cardiovasc Genet* 7(1):23–32.
19. May D, et al. (2011) Large-scale discovery of enhancers from human heart tissue. *Nat Genet* 44(1):89–93.
20. Wang J, et al. (2013) MicroRNA-17-92, a direct Ap-2α transcriptional target, modulates T-box factor activity in orofacial clefting. *PLoS Genet* 9(9):e1003785.
21. Dobrzynski H, Boyett MR, Anderson RH (2007) New insights into pacemaker activity: Promoting understanding of sick sinus syndrome. *Circulation* 115(14):1921–1932.
22. Lee JM, Kalman JM (2013) Sinus node dysfunction and atrial fibrillation: Two sides of the same coin? *Europace* 15(2):161–162.
23. Sairaku A, et al. (2012) Prediction of sinus node dysfunction in patients with long-standing persistent atrial fibrillation using the atrial fibrillatory cycle length. *J Electrocardiol* 45(2):141–147.
24. Risebro CA, et al. (2012) Epistatic rescue of Nkx2.5 adult cardiac conduction disease phenotypes by prospero-related homeobox protein 1 and HDAC3. *Circ Res* 111(2):e19–e31.
25. Chen J, et al. (2013) mir-17-92 cluster is required for and sufficient to induce cardiomyocyte proliferation in postnatal and adult hearts. *Circ Res* 112(12):1557–1566.
26. Hoogaars WM, et al. (2007) Tbx3 controls the sinoatrial node gene program and imposes pacemaker function on the atria. *Genes Dev* 21(9):1098–1112.
27. Blaschke RJ, et al. (2007) Targeted mutation reveals essential functions of the homeodomain transcription factor Shox2 in sinoatrial and pacemaking development. *Circulation* 115(14):1830–1838.
28. Puskaric S, et al. (2010) Shox2 mediates Tbx5 activity by regulating Bmp4 in the pacemaker region of the developing heart. *Hum Mol Genet* 19(23):4625–4633.
29. Bressan M, Liu G, Mikawa T (2013) Early mesodermal cues assign avian cardiac pacemaker fate potential in a tertiary heart field. *Science* 340(6133):744–748.
30. Yi T, et al. (2012) Electrophysiological mapping of embryonic mouse hearts: Mechanisms for developmental pacemaker switch and internodal conduction pathway. *J Cardiovasc Electrophysiol* 23(3):309–318.
31. Liu H, et al. (2012) The role of Shox2 in SAN development and function. *Pediatr Cardiol* 33(6):882–889.
32. Pfeufer A, et al. (2010) Genome-wide association study of PR interval. *Nat Genet* 42(2):153–159.
33. Bakker ML, et al. (2012) T-box transcription factor TBX3 reprogrammes mature cardiac myocytes into pacemaker-like cells. *Cardiovasc Res* 94(3):439–449.
34. Danielson LS, et al. (2012) Cardiovascular dysregulation of miR-17-92 causes a lethal hypertrophic cardiomyopathy and arrhythmogenesis. *FASEB J* 27(4):1460–1467.
35. Lu Y, et al. (2010) MicroRNA-328 contributes to adverse electrical remodeling in atrial fibrillation. *Circulation* 122(23):2378–2387.
36. Adam O, et al. (2012) Role of miR-21 in the pathogenesis of atrial fibrosis. *Basic Res Cardiol* 107(5):278.
37. Cardin S, et al. (2012) Role for MicroRNA-21 in atrial profibrillatory fibrotic remodeling associated with experimental postinfarction heart failure. *Circ Arrhythm Electrophysiol* 5(5):1027–1035.
38. Dawson K, et al. (2013) MicroRNA29: A mechanistic contributor and potential biomarker in atrial fibrillation. *Circulation* 127(14):1466–1475, 1475e1-28.
39. Harada M, et al. (2012) Transient receptor potential canonical-3 channel-dependent fibroblast regulation in atrial fibrillation. *Circulation* 126(17):2051–2064.
40. Luo X, et al. (2013) MicroRNA-26 governs profibrillatory inward-rectifier potassium current changes in atrial fibrillation. *J Clin Invest* 123(5):1939–1951.
41. Liu Z, et al. (2012) The expression levels of plasma micoRNAs in atrial fibrillation patients. *PLoS ONE* 7(9):e44906.
42. Xiao J, et al. (2011) MicroRNA expression signature in atrial fibrillation with mitral stenosis. *Physiol Genomics* 43(11):655–664.
43. Wahlquist C, et al. (2014) Inhibition of miR-25 improves cardiac contractility in the failing heart. *Nature* 508(7497):531–535.
44. Gore-Panter SR, et al. (2014) Atrial Fibrillation associated chromosome 4q25 variants are not associated with PITX2c expression in human adult left atrial appendages. *PLoS ONE* 9(1):e86245.
45. George SH, et al. (2007) Developmental and adult phenotyping directly from mutant embryonic stem cells. *Proc Natl Acad Sci USA* 104(11):4455–4460.
46. Respress JL, et al. (2012) Role of RyR2 phosphorylation at S2814 during heart failure progression. *Circ Res* 110(11):1474–1483.
47. Li N, et al. (2012) Inhibition of CaMKII phosphorylation of RyR2 prevents induction of atrial fibrillation in FKBP12.6 knockout mice. *Circ Res* 110(3):465–470.
48. Sood S, et al. (2008) Intracellular calcium leak due to FKBP12.6 deficiency in mice facilitates the inducibility of atrial fibrillation. *Heart Rhythm* 5(7):1047–1054.
49. Chelu MG, et al. (2009) Calmodulin kinase II-mediated sarcoplasmic reticulum Ca2+ leak promotes atrial fibrillation in mice. *J Clin Invest* 119(7):1940–1951.